Moist Baroclinic Instability in the Presence of Surface–Atmosphere Coupling

WEIDONG JIANG AND WILLIAM J. GUTOWSKI JR.

Department of Geological and Atmospheric Sciences, Iowa State University, Ames, Iowa

(Manuscript received 21 September 1998, in final form 14 June 1999)

ABSTRACT

The influence of convective heating on baroclinic instability in the presence of surface sensible heat and moisture fluxes is investigated. Following previous numerical work, a two-dimensional continuous model on an f plane incorporates diabatic heating effects due to cumulus convection and surface sensible heat flux using parameterizations based on a wave-induced unstable boundary layer and associated moist convective destabilization. The temperature-damping effect of surface sensible heat flux is assumed to decrease exponentially with height, and the vertical distribution of convective heating uses a prescribed profile. The atmosphere is assumed to overlie an oceanic surface. In this configuration, convective heating occurs in the wave's cold sector.

General forms of the dispersion relation and eigenfunction are derived analytically. Results show that the most unstable wave is modified by the effect of convective latent heating. With weak convection, the wave's structure does not change much, while the wave's energy generation is hampered by the negative contribution of convection. In the presence of moderate convective heating, although the wave's energy generation is decreased by convection, the wave adjusts its structure to minimize the negative effect of convection and retain growth. In the region with strong convective heating, convective heating significantly changes the wave's temperature structure. Above and below the strong heating region, the wave structure still retains some features of the Eady mode. The results have bearing on how the structure of oceanic storms may be altered by convection.

1. Introduction

Large-scale atmospheric eddies can be satisfactorily explained by baroclinic instability theory, which was elegantly introduced in analytical studies by Charney (1947) and Eady (1949). Observational and numerical studies have shown the importance to these eddies of latent heat released by condensation, so many studies that have since been done have incorporated convective heating into dry baroclinic instability theory (e.g., Tokioka 1973; Mak 1982, 1983, 1994; Wang and Barcilon 1986; Bannon 1986; Moorthi and Arakawa 1985; Emanuel et al. 1987; Fantini 1990; Balasubramanian and Yau 1994). Although there exist some differences among these studies [e.g., Moorthi and Arakawa (1985) examined moist baroclinic instability in easterly flow], these studies generally show that convection tends to increase growth rates of the most unstable waves and shift the wavelength of maximum instability toward shorter waves.

A common assumption in most of these analytical studies is that low-level convergence organizes the location and horizontal extent of convection. The degree of low-level convergence in these studies is measured by the large-scale, low-level vertical motion generated by the wave either by itself or in conjunction with Ekman pumping. In studies of slantwise convection by Emanuel et al. (1987) and Fantini (1990), this assumption is modified slightly to a requirement that at each level in the atmosphere, the location of the wave's upward motion determines where moist convective effects modify the large-scale flow. In these analytical studies, convective heating is vertically distributed by a specified profile. None of the studies cited above includes the influence of surface sensible heat flux, although some studies do consider the effect of surface momentum flux (friction).

With a primitive equation, global spectral model, Gutowski and Jiang (1998) (hereafter referred to as GJ) performed eddy life cycle simulations for the case of an idealized aquaplanet, focusing on the interaction of convection and baroclinic waves with and without surface fluxes included. In their numerical simulations, whether or not surface fluxes were included in the model had a crucial effect on the location of convection and its interaction with the wave. Results using different convection schemes (Kuo, Grell, Emanuel) all demonstrated that the determining characteristic for locating wave-induced convection during the linear growth stage was where the wave induced an unstable planetary boundary layer (PBL). This was because the temperature and moisture profiles created in the unstable PBL

Corresponding author address: Dr. Weidong Jiang, Litton PRC, Inc., 1500 PRC Drive, Mail Stop 2W3, McLean, VA 22102.
E-mail: Jiang_Weidong@prc.com

destabilized the atmosphere with respect to moist convection. The horizontal distribution of destabilization was modulated by the horizontal structure of the baroclinic wave.

With no surface interaction, the unstable boundary layer and convection were in the wave's warm sector. Adding surface fluxes caused the unstable PBL to be located in the wave's cold sector. For this case in particular, surface sensible and latent heat fluxes associated with the unstable PBL helped destabilize the atmosphere with respect to moist convection. Thus, when surface fluxes were included, moist convection occurred as a direct response to convective destabilization in the wave's cold sector. This behavior in itself was independent of convection scheme used and thus was why the same distribution of convection occurred in GJ's numerical simulations irrespective of convection parameterization. The convection in these cases was shallow because there was no large-scale support for deep convection.

For flow over an ocean surface, strong surface sensible heat flux and moisture flux are induced by cold and dry air flowing over a relatively warm and wet surface. Thus, a wave-induced unstable PBL and shallow convection often occur in the wave's cold sector as a response to the surface fluxes' heating and moistening. This behavior is often observed in winter cyclones over the ocean (Olafsson and Okland 1994). Some studies have shown that surface sensible heat flux by itself can cause diabatic destabilization in the atmosphere near the lower boundary and support unstable baroclinic waves, though only if they are short (meso-α) wavelengths (Orlanski 1986; Fantini 1995; Mak 1998).

To understand better the effect of an unstable PBL in helping to organize the distribution of wave-induced convection, we perform here an analytical study, suggested by GJ, of baroclinic instability in the presence of surface–atmosphere coupling. Such an analytical study can examine wave instability for a wide range of wavenumbers, which would not be practical for numerical studies. Following the aquaplanet assumption used in GJ, we assume that a growing wave moves cold and dry air over a relatively warm and wet surface. As a consequence, strong surface sensible heat and moisture fluxes are induced in the wave's cold sector, causing an unstable PBL. (The cold sector also has equatorward wind and negative eddy temperature.) Motivated by the behavior described in GJ, in this study, the effects of surface sensible heat flux and convective heating rate are linked to near-surface eddy temperature. Convection is then specifically located in the wave's cold sector, with the convective heating rate parameterized in terms of the degree of PBL destabilization, which we assume is proportional to the magnitude of the near-surface (negative) eddy temperature, as in GJ (e.g., their Fig. 7). We assume that sufficient surface moisture flux for moist convection occurs, as it did in GJ. The parameterization distinguishes this study from previous analytical studies of moist convection and baroclinic instability that did not include surface energy fluxes. For simplicity the Eady model instead of the Charney model is used in this study since the absence of β effect does not change the fundamental features of instability (Mak 1983).

2. Model formulation

a. Basic equations

Following previous studies by Mak (1982, 1994) and Wang and Barcilon (1986), the model used in this study is a two-dimensional Eady model with a boundary layer coupled to a surface that allows for disturbance-induced convection. The governing perturbation equations for vorticity and temperature may be written in nondimensional form as

$$\left(\frac{\partial}{\partial t} + U\frac{\partial}{\partial x}\right)\frac{\partial^2\psi}{\partial x^2} = \frac{\partial\omega}{\partial p}, \tag{1}$$

$$\left(\frac{\partial}{\partial t} + U\frac{\partial}{\partial x}\right)\frac{\partial\psi}{\partial p} + \lambda\frac{\partial\psi}{\partial x} + \sigma\omega = -\frac{Q}{p}, \tag{2}$$

where ψ is the perturbation streamfunction and ω is the perturbation vertical velocity. The zonally averaged basic state, $U = \lambda(1 - p)$, has constant vertical wind shear λ and basic static stability σ. The term Q, on the right-hand side of (2), is nondimensional diabatic heating rate. Other symbols have their conventional meteorological definitions.

The model domain is expressed in the nondimensional form as $0 \le x < \infty$, $p_U \le p \le p_L$, and the vertical boundary conditions are

$$\omega = 0 \quad \text{at } p = p_U, p_L, \tag{3}$$

where p_U and p_L represent the nondimensional pressure values at the upper and lower boundaries of the model atmosphere, respectively.

This is a boundary value problem with two equations and three unknowns: perturbation streamfunction ψ, perturbation vertical velocity ω, and diabatic heating rate Q. To solve the problem, we need to parameterize Q in terms of the wave's variables.

b. Treatment of the diabatic heating

As discussed in the introduction, when the atmosphere is coupled to an oceanlike (high heat capacity) surface, the wave induces strong surface sensible heat flux and moisture flux where cool air flows over a relatively warm surface, so that an unstable PBL and, hence, moist convective destabilization can occur in the wave's cold sector. Although this is a region of large-scale descending motion, substantial surface moisture and sensible heat flux are assumed capable of providing the necessary convective destabilization to provoke shallow convection despite the lack of large-scale lift-

ing, as occurred in GJ. The scenario presents a wave-convection coupling different from the concept of conditional instability of the second kind (CISK). In accordance with the scenario and consistent with our earlier numerical findings, we also assume that the PBL damps the temperature wave by surface sensible heat flux.

Following previous linear studies (Mak 1982; Bannon 1986; Wang and Barcilon 1986; Mak 1994), the convective heating is assumed to be distributed vertically according to a specified heating profile. In contrast to prior studies, we do not link convective heating to eddy vertical velocity. Rather, in this study, the convective heating rate is assumed to be proportional to the degree of moist convective destabilization produced by an unstable PBL and associated surface sensible and latent heat fluxes. Following the results of GJ, we assume that the surface fluxes are proportional to near-surface eddy temperature. More specifically, we assume that the convective heating rate is proportional to the rate of destabilization and thus proportional to eddy temperature at a certain level p_m, which is approximately the top of the unstable PBL. This assumption is based on the consideration that the degree of PBL instability is proportional to the temperature difference between the surface and the top of the PBL. The convective heating tendency is thus assumed to be a quasi-equilibrium response to convective destabilization by wave-induced surface fluxes (cf., Emanuel 1991). Hereafter, this scheme is referred to as the *T*-parameterization scheme.

The diabatic heating rate due to convection can then be expressed as

$$Q_1 = -\varepsilon_T \eta(p) T(p_m), \tag{4}$$

where T denotes eddy temperature, and the vertical heating profile is represented by $\eta(p)$. The convective heating intensity parameter ε_T has a dimension of inverse seconds. For a positive heating intensity parameter, a wave induces heating where the eddy temperature is negative (the cold sector of a wave). At the same time, convective cooling exists in the warm sector of a wave. This unconditional convective heating and cooling that exists across the wave gives mathematical convenience and may be viewed simply as the contribution to the heating from the fundamental harmonic component (Mak 1982, 1994; Bannon 1986). The use of a convective parameterization without the cooling is not practical in such linear studies, since it leads to a Fourier series expansion in space that couples modes of different spatial scales (Lindzen 1974).

We also include the diabatic heating due to surface sensible heat flux. Surface sensible heat flux tends to suppress the amplitude of the temperature wave near the surface, so the diabatic heating rate due to surface sensible heat flux is assumed to be a damping term proportional to eddy temperature at the level p_m,

$$Q_2 = -\gamma \xi(p) T(p_m), \tag{5}$$

where the damping intensity parameter γ, like ε_T, has a dimension of inverse seconds, and the vertical damping profile is specified by $\xi(p)$. If $\gamma > 0$, surface sensible heat flux heats the wave's cold sector and cools the wave's warm sector, so it directly damps the temperature wave. For brevity, we will sometimes call it the surface-flux damping term. The parameterization of surface sensible heat flux is similar to that used in Mak (1998), where surface sensible heat flux is related to the eddy temperature field at the lower boundary.

In terms of the hydrostatic and quasigeostrophic relations, (4) and (5) can be rewritten in nondimensional form as

$$Q_1 = \varepsilon_T \eta(p) \frac{f\psi(p_m)}{fp} \quad \text{and} \tag{4'}$$

$$Q_2 = \gamma \xi(p) \frac{f\psi(p_m)}{fp}. \tag{5'}$$

Then, the diabatic heating rate Q can be expressed as

$$Q = Q_1 + Q_2. \tag{6}$$

Using the above parameterization of diabatic heating, the unknowns in the system are reduced to only the perturbation streamfunction ψ and the perturbation vertical velocity ω.

We express a wave mode of the solution as the normal mode

$$(\omega, \psi) = [\Omega(p), \Psi(p)] e^{ik(x-ct')},$$

where $i = \sqrt{-1}$, k is the wavenumber, and c is the complex phase speed. The amplitude functions $\Omega(p)$ and $\Psi(p)$ are also complex. Substituting the normal mode into (1), (2), (4′), and (5′) and eliminating Ψ in favor of Ω, we obtain the equation that governs the amplitude function $\Omega(p)$:

$$\begin{aligned}\frac{d^2\Omega}{dp^2} + \frac{2\lambda}{U(p) - c}\frac{d\Omega}{dp} - k^2\sigma\Omega \\ = \frac{i\varepsilon_T p_m \eta(p)}{kp[U(p_m) - c]^2}\left[[U(p_m) - c]\frac{d^2\Omega(p_m)}{dp^2} + \lambda\frac{d\Omega(p_m)}{dp}\right] \\ + \frac{i\gamma p_m \xi(p)}{kp[U(p_m) - c]^2} \\ \times \left[[U(p_m) - c]\frac{d^2\Omega(p_m)}{dp^2} + \lambda\frac{d\Omega(p_m)}{dp}\right].\end{aligned} \tag{7}$$

The boundary conditions now become

$$\text{Upper:} \quad \Omega = 0 \quad \text{at } p = p_U \quad \text{and} \tag{8}$$

$$\text{Lower:} \quad \Omega = 0 \quad \text{at } p = p_L. \tag{9}$$

We require the perturbation vertical velocity ω and perturbation streamfunction ψ to be continuous at cloud base and top, which imposes internal conditions at the cloud boundaries:

Ω and $\dfrac{d\Omega}{dp}$ are continuous at cloud base p_B and cloud top p_T. (10)

The system consisting of (7)–(10) formulates an eigenvalue problem for the complex phase speed c.

c. General eigenvalue problem and its solution

Following Wang and Barcilon (1986), the solution to the above general eigenvalue problem can be obtained using the method of variation of parameters. Because the two forcing terms have different vertical profiles, we solve the system by applying the method of variation of parameters twice, which is different from Wang and Barcilon (1986). Outside the cloud region, the solution reduces to the modified Eady solution in the presence of surface-flux damping. When convective heating and surface-flux damping are all zero, the solution reduces to the Eady solution.

First, applying the method of variation of parameters to (7) without convective heating ($\varepsilon_T = 0$), we get two linearly independent solutions:

$$g_1(p) = [A_1(p) + 1]f_1(p) + B_1(p)f_2(p) \quad (11a)$$

$$g_2(p) = A_1(p)f_1(p) + [B_1(p) + 1]f_2(p), \quad (11b)$$

where two homogeneous solutions, $f_1(p)$ and $f_2(p)$, are in the same form as (3.6a) and (3.6b) in Wang and Barcilon with $r = 0$. Thus,

$$f_1(p) = \Omega_2(p_L)\Omega_1(p) - \Omega_1(p_L)\Omega_2(p) \quad (12a)$$

$$f_2(p) = \Omega_2(p_U)\Omega_1(p) - \Omega_1(p_U)\Omega_2(p), \quad (12b)$$

where $\Omega_1(p)$ and $\Omega_2(p)$ are two fundamental solutions of the Eady case. Readers are referred to Wang and Barcilon (1986) for detailed derivation of $f_1(p)$ and $f_2(p)$. Other symbols in (11a) and (11b) are

$$A_1(p) = \frac{i\gamma p_m}{kf_1(p_U)F^2(p_m)}\left[F(p_m)\frac{d^2\Omega_s(p_m)}{dp^2} + \lambda\frac{d\Omega_s(p_m)}{dp}\right] \times \int_{p_U}^{p}\frac{\xi(t)f_2(t)}{tW(t)}\,dt \quad (13a)$$

$$B_1(p) = \frac{-i\gamma p_m}{kf_1(p_U)F^2(p_m)}\left[F(p_m)\frac{d^2\Omega_s(p_m)}{dp^2} + \lambda\frac{d\Omega_s(p_m)}{dp}\right] \times \int_{p_L}^{p}\frac{\xi(t)f_1(t)}{tW(t)}\,dt, \quad (13b)$$

where $F(p) = U(p) - c$,

$$W(p) = \Omega_1(p)\Omega_2'(p) - \Omega_1'(p)\Omega_2(p), \quad (14)$$

and the subscript s denotes the solution for surface damping only. Hereafter, the prime denotes a derivative with respect to pressure p. The Wronskian for g_1 and g_2,

$$W_R(g_1, g_2; p) = -f_1(p_U)[A_1(p) + B_1(p) + 1]W(p), \quad (15)$$

is not equal to zero in the presence of diabatic heating because $f_1(p)$ and $f_2(p)$ are linearly independent.

Then, in terms of $g_1(p)$ and $g_2(p)$, we apply the method of variation of parameters to (7). The following dispersion equation can be obtained (Jiang 1998):

$$D_1 f_1(p_U) - \frac{i\varepsilon_T p_m}{kF^2(p_m)}\left[F(p_m)\frac{d^2\Omega(p_m)}{dp^2} + \lambda\frac{d\Omega(p_m)}{dp}\right] \times [I_2(p_B) - I_2(p_T)] = 0. \quad (16)$$

The eigenfunction is given by

$$\Omega(p) = \begin{cases} D_1 g_1(p), & p_L \geq p > p_B \\ A_2(p)g_1(p) + B_2(p)g_2(p), & p_B \geq p \geq p_T \\ D_2 g_2(p), & p_T > p \geq p_U, \end{cases} \quad (17)$$

where D_1 is an arbitrary constant and

$$A_2(p) = \frac{i\varepsilon_T p_m}{kf_1(p_U)F^2(p_m)}\left[F(p_m)\frac{d^2\Omega(p_m)}{dp^2} + \lambda\frac{d\Omega(p_m)}{dp}\right] \times [I_2(p) - I_2(p_T)], \quad (18a)$$

$$B_2(p) = \frac{i\varepsilon_T p_m}{kf_1(p_U)F^2(p_m)}\left[F(p_m)\frac{d^2\Omega(p_m)}{dp^2} + \lambda\frac{d\Omega(p_m)}{dp}\right] \times [I_1(p_B) - I_1(p)], \quad (18b)$$

$$D_2 = \frac{i\varepsilon_T p_m}{kf_1(p_U)F^2(p_m)}\left[F(p_m)\frac{d^2\Omega(p_m)}{dp^2} + \lambda\frac{d\Omega(p_m)}{dp}\right] \times [I_1(p_B) - I_1(p_T)]. \quad (18c)$$

Furthermore,

$$\frac{d^2\Omega(p_m)}{dp^2} = D_1\frac{H_1(p_m)g_1''(p_m) + i\varepsilon_T\lambda H_2(p_m)g_1'(p_m)}{H_1(p_m) - i\varepsilon_T F(p_m)H_2(p_m)}, \quad (19)$$

$$\frac{d\Omega(p_m)}{dp} = \left[D_1 kf_1(p_U)F^2(p_m)g_1'(p_m) + i\varepsilon_T p_m I(p_m)F(p_m)\frac{d^2\Omega(p_m)}{dp^2}\right] \div H_1(p_m), \quad (20)$$

$$I_1(p) = \int^{p}\frac{\eta(t)g_1(t)}{tW(t)[A_1(t) + B_1(t) + 1]}\,dt, \quad (21a)$$

$$I_2(p) = \int^{p}\frac{\eta(t)g_2(t)}{tW(t)[A_1(t) + B_1(t) + 1]}\,dt, \quad (21b)$$

$$I(p) = g_2'(p)[I_1(p_B) - I_1(p)] - g_1'(p)[I_2(p_B) - I_2(p)], \quad (22a)$$

$$J(p) = g_2''(p)[I_1(p_B) - I_1(p)] - g_1''(p)[I_2(p_B - I_2(p)], \quad (22b)$$

$$H_1(p) = kf_1(p_U)F^2(p) - i\varepsilon_T\lambda pI(p), \quad (23a)$$

$$H_2(p) = pJ(p) - \eta(p)f_1(p_U). \quad (23b)$$

Detailed derivation of this section can be found in Jiang (1998). For convenience, the arbitrary constant D_1 is set to 1. It can be seen that when convective heating is absent ($\varepsilon_T = 0$), the dispersion equation (16) reduces to $f_1(p_U) = 0$. It is straightforward to show that $f_1(p_U) = 0$ or $f_2(p_L) = 0$ gives the Eady solution. Outside the cloud region, the eigenfunction equation (17) is the same as that with the surface-flux damping only.

3. Model results and analysis

a. Model parameters and vertical profiles

Given the basic state [$U(p)$ and $\sigma(p)$], the intensity parameters (ε_T and γ), the vertical profiles [$\eta(p)$ and $\xi(p)$], and the two fundamental solutions of the Eady case, the dispersion equation (16) can be solved by iteration using the secant method in complex space. Once the complex phase speed c is obtained, the eigenfunction (17) can be computed. In the computations, the following values for the parameters are chosen to represent the atmosphere:

$$p_U = 150 \text{ hPa}, \quad p_T = 400 \text{ hPa}, \quad p_B = 900 \text{ hPa},$$
$$p_L = 1000 \text{ hPa}, \quad p_m = 900 \text{ hPa},$$
$$\lambda = 0.035 \text{ m s}^{-1} \text{ (hPa)}^{-1}, \quad \sigma = 0.04 \text{ m}^2 \text{ s}^{-2} \text{ (hPa)}^{-2},$$
$$f = 10^{-4} \text{ s}^{-1}.$$

Using the characteristic values $L = 10^6$ m, $P_0 = 1000$ hPa, and $V = \lambda P_0$ m s^{-1}, the nondimensional values of the above parameters would be

$$p_U = 0.15, \quad p_T = 0.4, \quad p_B = 0.9, \quad p_L = 1.0,$$
$$p_m = 0.9, \quad \lambda = 1.0, \quad \sigma = 4.0.$$

The nondimensional zonal flow now is $U(p) = 1 - p$.

In GJ, the convective heating rate in the wave's cold sector was about 0.2 K day^{-1} on day 7, during the linear growth phase, and 10 K day^{-1} on day 13, when the wave reached its maximum amplitude. In this study, values of the convective heating intensity parameter from 0.0001 to 5.0 are examined to test sensitivity to this parameter. The range is wide enough, since $\varepsilon_T = 0.33$ corresponds to 10 K day^{-1} for eddy temperature of 10 K. (In later sections, ε_T is rescaled so that $\varepsilon_T = 1.0$ corresponds to this heating rate.)

The nondimensional heating profile is specified as in Wang and Barcilon (1986):

$$\eta(p) = \begin{cases} 0, & p_B < p \le p_L \\ \dfrac{12}{(p_B - p_T)^4}[b(p_B - p)(p - p_T)^2 + (1 - b)(p_B - p)^2(p - p_T)], & p_T \le p \le p_B \\ 0, & p_U \le p < p_T, \end{cases} \quad (24)$$

where the shape parameter b can be chosen in [0, 1] to adjust the location of maximum heating in the cloud (see Fig. 2 in Wang and Barcilon 1986). In accordance with the result of GJ, the maximum heating is located in the lower part of the cloud by setting $b = 1$ in most of the computations. Note that the specified heating profile does not generate convective cooling outside the cloud region, which gives mathematical convenience and is justified by our previous numerical simulations. In GJ, cooling occurred between 700 and 800 hPa from saturated downdrafts in the Emanuel parameterization scheme. Turning off this cooling in numerical simulations had little effect on wave growth and energetics, so we do not include it here.

We assume the surface-flux damping decreases exponentially with height, and the nondimensional damping profile is specified as

$$\xi(p) = \frac{ae^{-a(1-p/p_L)}}{p_L[1 - e^{-a(1-p_U/p_L)}]}. \quad (25)$$

The parameter a controls how fast the surface damping decreases with height, and it is set so that the damping at the level p_m reduces to e^{-3} of the surface value. For damping intensity parameter $\gamma = 1.0$, sensible heat flux is 100 W m^{-2} at 1 km above the surface, when surface eddy temperature is about 10 K.

Two fundamental solutions of the Eady case are

$$\Omega_1(p) = \frac{1}{\sqrt{2}}e^{\mu(1-p-c)}[\mu(1 - p - c) - 1]$$

$$\Omega_2(p) = \frac{1}{\sqrt{2}}e^{-\mu(1-p-c)}[\mu(1 - p - c) + 1],$$

where $\mu = \sigma^{1/2}k$. Then, we know that

$$W(p) = \Omega_1(p)\Omega_2'(p) - \Omega_2(p)\Omega_1'(p)$$
$$= \mu^3(1 - p - c)^2,$$

and two homogeneous solutions $f_1(p)$ and $f_2(p)$ are obtained:

$$f_1(p) = \mu(p_L - p)\cosh[\mu(p_L - p)] - [\mu^2(c - 1 + p_L)(1 - p - c) + 1] \times \sinh[\mu(p_L - p)]$$

$$f_2(p) = \mu(p_U - p)\cosh[\mu(p_U - p)] - [\mu^2(c - 1 + p_U)(1 - p - c) + 1] \times \sinh[\mu(p_U - p)].$$

One can now solve the dispersion equation [Eq. (16)] by iteration.

b. Comments about the solution to the eigenvalue problem

To consider the effect of convective heating, the domain is divided vertically into three regions, and the method of variation of parameters is applied to solve the system. Because it is not practical to get exact analytical solutions from the dispersion equation, we do not know how many solutions exist. We apply the following numerical procedure to search for solutions. The dispersion equation is solved numerically by iteration in complex phase speed space, where initial guess values are scanned through [0, 1] for the real part and [−0.15, 0.15] for the imaginary part. When computing the dispersion relation, for each parameter setting, the wavenumber of the normal mode is scanned from 0.001 to 10, with the increment 0.001. For small heating intensity parameters, a pair of complex conjugates (0.425, ±0.154) is found in the solutions, which is clearly the Eady solution recovered in the moist system. Compared to the Eady model, the system has some other mathematical solutions that are stable with the weak convective heating. These stable solutions are presumably due to the numerical computation of the integrals $I(p)$ and $J(p)$. In the iterative computation, these integrals are numerically computed, using the trapezoidal rule, by discretizing the continuous domain into 100 levels. The continuous problem has a continuous spectrum of neutral waves, but the discretizing approximation could generate a discretized spectrum of neutral waves (Farrell 1982). Because our focus is the effect of convective heating on baroclinically growing waves, we only examine the variation of the Eady-type modes with convective heating.

c. Analysis

Figure 1 gives the growth rate as a function of wavenumber for different heating intensities. We can see first that Eady's results are recovered when heating is negligible. As the heating parameter ε_T increases, the growth rate of unstable waves initially decreases and then increases, and the wavenumber of the most unstable wave shifts toward the short-wave cutoff. With strong heating, the maximum growth rate increases to a value equal to or larger than the Eady solution's maximum. The phase speed increases as the heating parameter ε_T increases (not shown). Note that some oscillations exist in the growth rate for large wavenumbers and large ε_T. In Jiang (1998), the growth rate change as ε_T increases was examined for spurious numerical behavior. At large wavenumbers and large ε_T, the near-neutral growth rate indicated some sensitivity in numerics to small parameter changes.

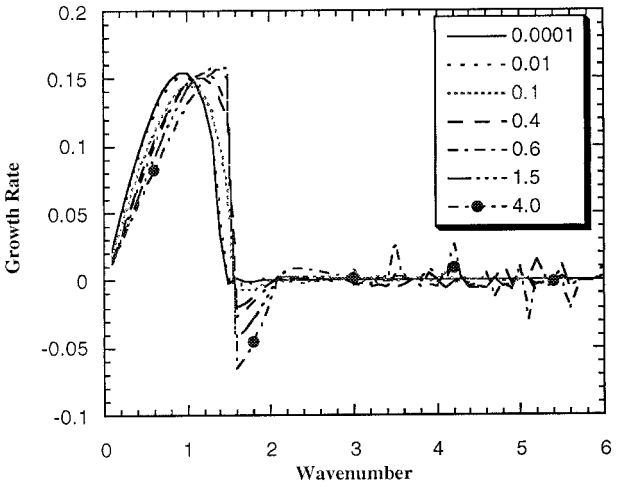

FIG. 1. Result of the *T*-parameterization model: variations of the growth rate, with the wavenumber for different heating intensities shown in key.

Figure 2 shows vertical structure variations of vertical velocity Ω when convective heating changes. One must keep in mind that the eigenfunctions have been arbitrarily normalized by choosing $D_1 = 1$ in (17). Therefore, it is meaningless to compare the absolute value of all eigenfunctions, and only the structures are unique and meaningful (Mak 1994). In Fig. 2a, the structure of the amplitude and phase angle barely changes with ε_T for weak heating ($\varepsilon_T < 0.01$), but the level of maximum amplitude rises into the upper atmosphere as ε_T increases to 0.1. The phase angle decreases substantially as $\varepsilon_T \rightarrow 0.1$ (Fig. 2).

The vertical structure of streamfunction Ψ varies with convective heating, as shown in Fig. 3. When $\varepsilon_T = 0.1$, the level of minimum amplitude shifts toward the lower atmosphere (Fig. 3a). In Fig. 3b, the phase angle decreases as the heating parameter ε_T increases. When heating is small ($\varepsilon_T < 0.01$), the structure of amplitude and phase angle changes little with ε_T.

Figure 4 shows the variations in the vertical structure of the wave's temperature T when the heating parameter ε_T changes. In Fig. 4a, the temperature amplitude increases with height between the level with maximum

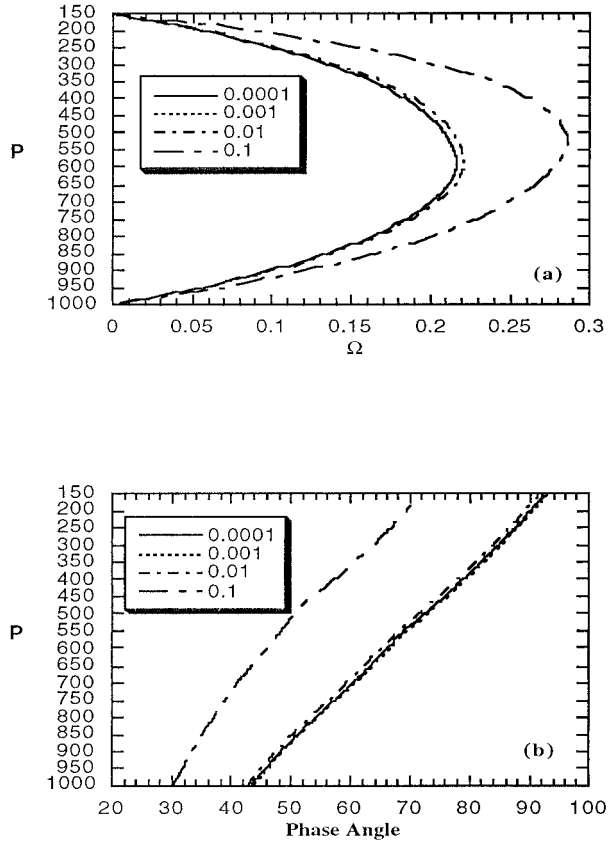

FIG. 2. Result of the *T*-parameterization model: the vertical structure of the vertical velocity (a) amplitude Ω and (b) phase angle for wavenumber $k = 0.9$ for different heating intensities ε_T.

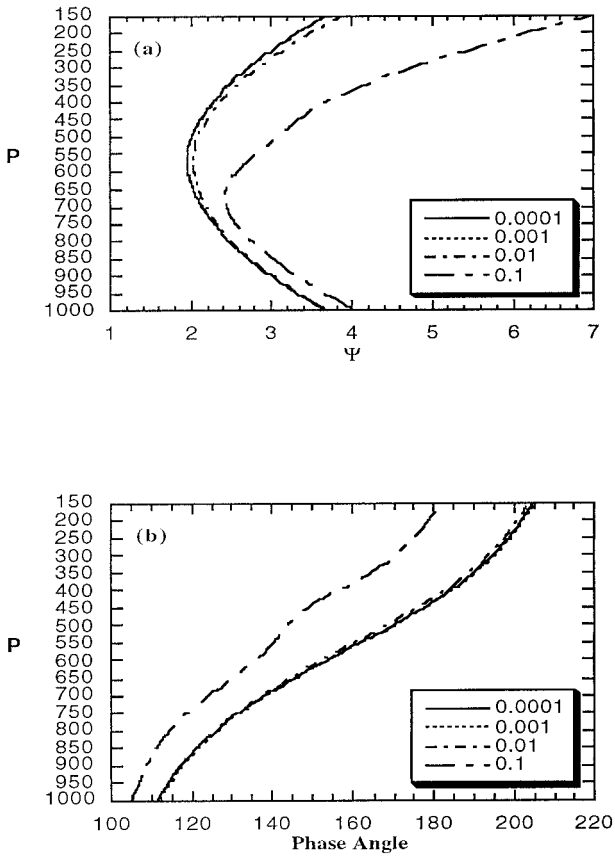

FIG. 3. Result of the *T*-parameterization model: the vertical structure of the streamfunction (a) amplitude Ψ and (b) phase angle for wavenumber $k = 0.9$ for different heating intensities ε_T.

heating and the cloud top when $\varepsilon_T = 0.1$. With the same heating intensity ($\varepsilon_T = 0.1$), the structure of the phase angle changes so much that the temperature wave tilts more eastward, between 900 and 600 hPa, but more westward, between 600 and 400 hPa (Fig. 4b). In the lower atmosphere, the phase angle change with heating intensity is negligible. Similarly, we can see little change in the structure of amplitude and phase angle with small convective heating.

Why wave structure changes can be seen more clearly in vertical–horizontal cross-section plots. As a reference state for comparison, Fig. 5 shows the eigenfunction cross sections of vertical velocity, streamfunction, and temperature for the Eady case. The vertical velocity and streamfunction fields are vertically symmetric and tilt westward with height. The temperature field tilts eastward with height, and its amplitude decreases with height. When heating intensity increases to 0.1, the change in the vertical velocity field is not visible in Fig. 6a, but the streamfunction field becomes asymmetric, and a local center develops near 700 hPa (Fig. 6b). Figure 6c clearly shows structure modification in the temperature wave by convective heating. In the region with strong convective heating, the warm sector nudges horizontally into the cold sector, with the opposite behavior where there is convective cooling. The behavior can be viewed as the result of superimposing convective heating (Fig. 6d) on the temperature field of the Eady case (Fig. 5c).

When heating intensity increases to 1.0, the structure change due to convective heating can be seen in vertical velocity, streamfunction, and temperature fields. Maximum vertical velocity now occurs in the upper atmosphere so that the vertical velocity field becomes vertically asymmetric (Fig. 7a). In the streamfunction field (Fig. 7b), the local center near 700 hPa increases further in amplitude between 600 and 900 hPa. In the temperature field (Fig. 7c), we see temperature wave patterns in three regions. Between 600 and 900 hPa, the wave structure differs from the Eady mode. Above or below this region, the wave structure still retains some features of the Eady mode, but it is modified because the vertical velocity is continuous at the new boundaries generated by strong convective heating. Convective heating significantly changes the wave's temperature structure, which again can be viewed approximately as a superpositioning of convective heating on the Eady case's wave temperature.

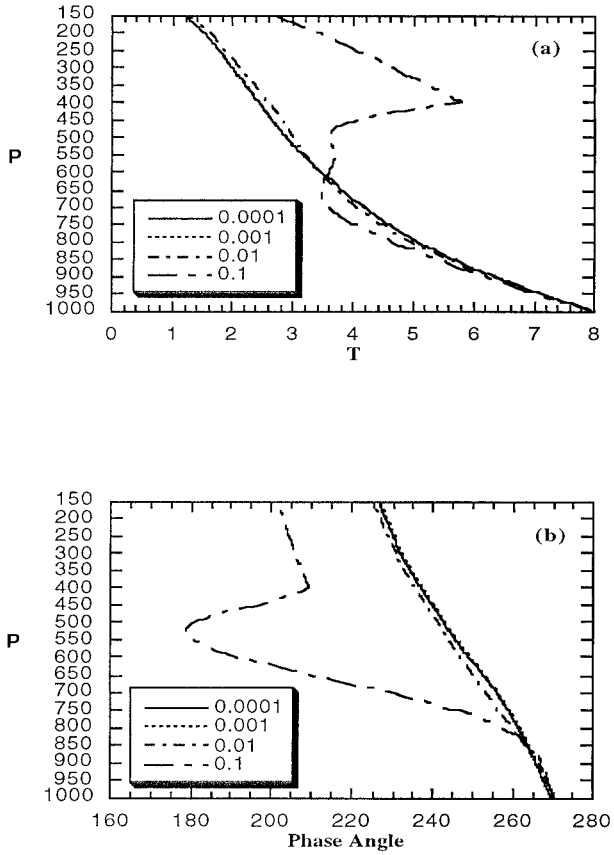

FIG. 4. Result of the *T*-parameterization model: the vertical structure of the temperature (a) amplitude *T* and (b) phase angle for wavenumber $k = 0.9$ for different heating intensities ε_T.

As we can see, the wave structure changes in presence of convective heating so that the phase relationship for growth existing in the Eady wave is not present with convective heating. Recall that for the Eady case, the temperature wave lags $\pi/4$ radians behind the geopotential height wave and π radians behind the vertical velocity wave in the p coordinate so that warm air ascends and cold air descends in the middle atmosphere, giving an optimal structure for converting eddy available potential energy (EPE) to eddy kinetic energy (EKE). Table 1 gives the phase angle difference, for different heating parameters, between the vertical velocity wave and the temperature wave at the level where vertical velocity amplitude reaches its maximum. When the convective heating parameter increases, the wave structure changes, and the warm (cold) region shifts away from the ascent (descent) motion region so that the wave does not convert EPE to EKE as effectively and thus cannot grow as fast as the Eady case. With further increase in ε_T, the phase angle difference increases. When $\varepsilon_T > 0.8$, the warm and cold regions again align with the ascent and descent motion regions.

To investigate the wave energetics, we analyze the energetic budget terms:

$$\mathrm{DIV[EE]} = -\left\langle \frac{f}{fp}(\omega\psi) \right\rangle,$$

$$\mathrm{C[EPE, EKE]} = \left\langle \omega \frac{f\psi}{fp} \right\rangle,$$

$$\mathrm{C[ZPE, EPE]} = -\frac{\lambda}{\sigma}\left\langle \frac{f\psi}{fx}\frac{f\psi}{fp} \right\rangle,$$

$$\mathrm{G[CONV]} = \frac{1}{\sigma}\left\langle \frac{f\psi}{fp}\frac{-Q_1}{p} \right\rangle,$$

$$\mathrm{G[DAMP]} = \frac{1}{\sigma}\left\langle \frac{f\psi}{fp}\frac{-Q_2}{p} \right\rangle,$$

where the angle brace denotes integration over the domain. The first term, DIV[EE], is the divergence of vertical wave–energy flux, and it goes to zero because divergence balances convergence due to the boundary conditions on ω. The second term, C[EPE, EKE], is the conversion rate from EPE to EKE. The third term, C[ZPE, EPE], is the conversion rate from zonal available potential energy (ZPE) to EPE. The last two terms, G[CONV] and G[DAMP], are the contributions of convective heating and surface-flux damping to the EPE generation.

Using $\Omega(p)$ and $\Psi(p)$, we can evaluate these energy budget terms. Figure 8 shows the vertical structure of the integrands for the energy budget terms for wavenumber $k = 0.9$ and $\varepsilon_T = 0.0001$. We can see the energy flow path of typical baroclinic waves: meridional motion converts ZPE to EPE and vertical motion converts EPE to EKE. While C[ZPE, EPE] is vertically uniform, the energy conversion C[EPE, EKE] has a maximum in the middle of the atmosphere where eddy vertical velocity is largest in magnitude. The energetic contribution of convective heating, G[CONV], is negligible, and the damping is confined mostly to the lower atmosphere.

Figure 9 shows the vertical structure of the integrands for the energy budget terms for wavenumber $k = 0.9$ for $\varepsilon_T = 0.1$. Above the cloud base, as we can see, the vertical distributions of DIV[EE], C[EPE, EKE], and C[ZPE, EPE] have changed relative to the Eady case. Variations in vertical structure of the energetic terms correspond to the variation of eigenfunction structure in the same vertical section (cf., Figs. 5, 6, and 7). However, the energy flow still follows the path of typical baroclinic waves, as in the Eady case: the eddy grows baroclinically, drawing energy from the ZPE reservoir and through the EPE reservoir.

Because the linear instability problem has arbitrary normalization, it is meaningless to compare the absolute values of the energy terms for different heating intensity. However, we can compare values of C[EPE, EKE], G[CONV], and G[DAMP] relative to C[ZPE, EPE]. In other words, we can compare the ratios

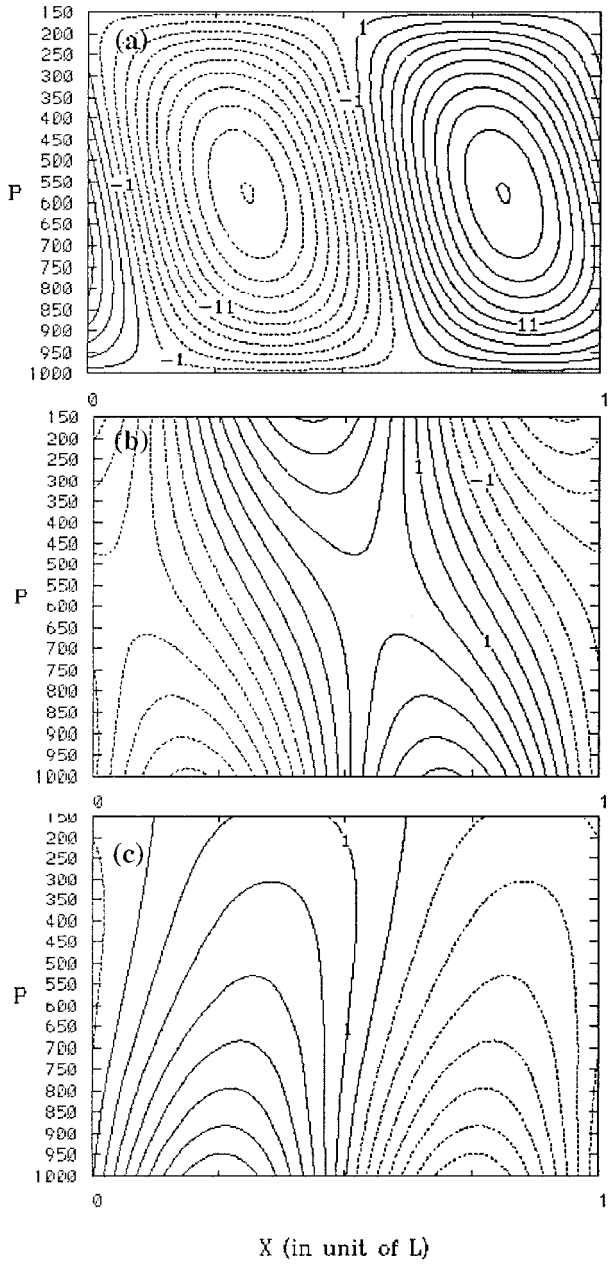

FIG. 5. Result of the *T*-parameterization model: the vertical–horizontal cross section of (a) vertical velocity ω, (b) streamfunction ψ, and (c) temperature T for wavenumber $k = 0.9$ for the Eady case ($\varepsilon_T = 0.0$).

$$\text{C*[EPE, EKE]} = \frac{\text{C[EPE, EKE]}}{\text{C[ZPE, EPE]}},$$

$$\text{G*[CONV]} = \frac{\text{G[CONV]}}{\text{C[ZPE, EPE]}},$$

$$\text{G*[DAMP]} = \frac{\text{G[DAMP]}}{\text{C[ZPE, EPE]}},$$

for different heating parameter ε_T (Fig. 10). As we can see, with weak heating ($\varepsilon_T < 0.2$), C[EPE, EKE] decreases while the negative contribution of convection increases in magnitude. For moderate heating ($0.2 < \varepsilon_T < 2.0$), the magnitude of G[CONV] decreases, consistent with the structural changes in the wave's temperature structure (e.g., Fig. 7). For $2.0 < \varepsilon_T < 3.0$, the effect of convective heating alters the wave's structure so much that G*[CONV] becomes weakly positive. When ε_T increases beyond 3.0, G[CONV] becomes negative again. With increasing ε_T in Fig. 10, the magnitude of G[DAMP] decreases toward zero. It is pertinent to point out here that the energy conversion C[ZPE, EPE] may also change in the presence of convective heating, but its variation with heating intensity cannot be seen in this analysis.

As we have seen, the wave's behavior has changed in the presence of the *T*-parameterization and surface damping. With weak convection, the wave's structure does not change much, while the EPE generation decreases due to the negative contribution of convection. In the presence of moderate convective heating, although the EPE generation still decreases, the wave's structure changes accordingly to minimize the negative effect of convection. The energetic contribution of convection becomes a small positive value when ε_T is about 2.0. The term G[CONV] becomes negative with further increases in heating.

d. Sensitivity experiments

Is the growing wave's behavior, delineated above, dependent on the convective parameterization? To investigate the sensitivity to the convective scheme, we performed similar analysis using an alternative approach, termed the v-parameterization scheme. For this parameterization, we assume the unstable PBL occurs where cold air flows equatorward. We thus assume that the degree of PBL destabilization, strength of surface heat flux, and moist convective destabilization is proportional to the v component. This occurs mostly in the cold sector of a wave, although the meridional wind is shifted horizontally, relative to the temperature wave. At the same time, convective cooling exists where wind has a poleward component (which is mostly in the warm sector of a wave). As it is known, surface sensible heat flux in its bulk representation is related to the wind speed near the surface as well as the surface–air temperature difference. In the v-parameterization scheme, the convective heating rate is assumed to be proportional to the v component of eddy velocity at the level p_m; that is,

$$Q_1 = -\varepsilon_v \eta(p) v(p_m), \tag{26}$$

where ε_v is the convective heating intensity parameter (units km^{-1}). The heating parameter $\varepsilon_v = 1.0$ corresponds to 4 K day^{-1} for a wind speed of 10 m s^{-1}. For the positive heating intensity parameter, a wave induces heating where wind is equatorward. This parameteri-

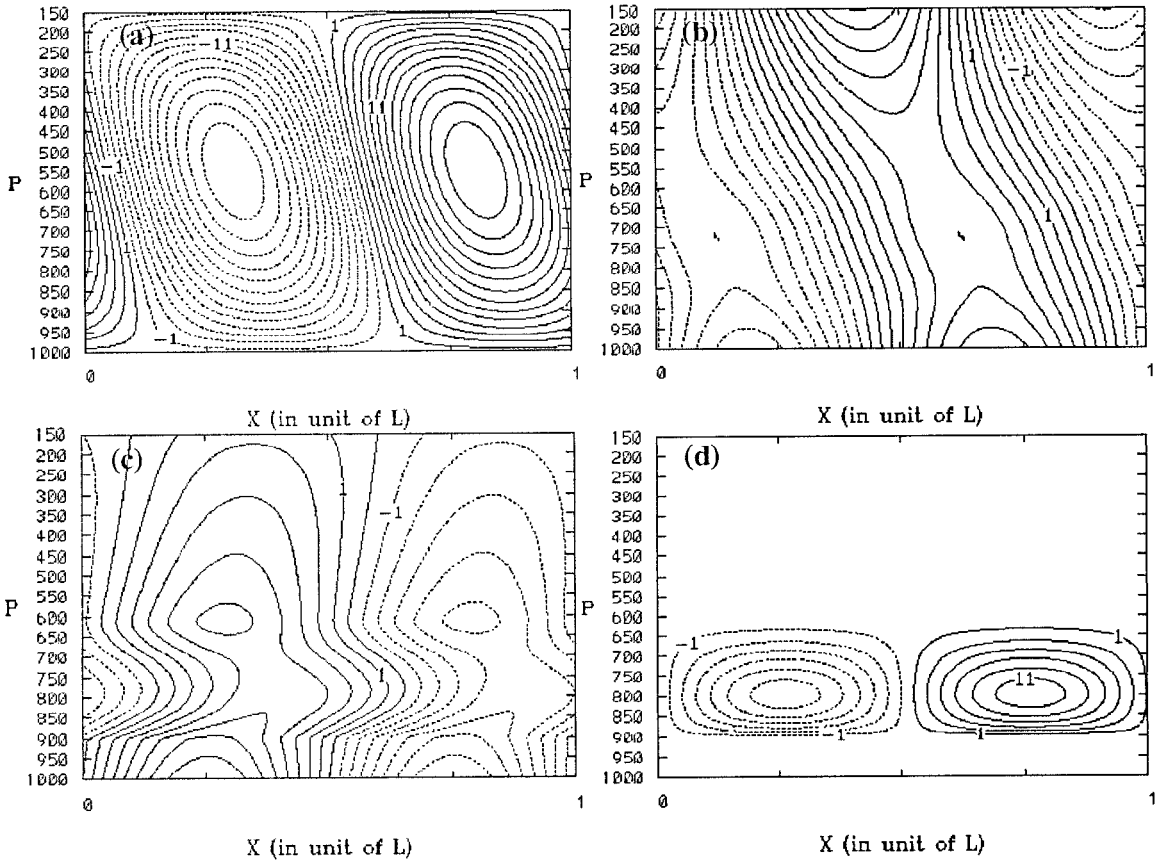

FIG. 6. Result of the *T*-parameterization model: the vertical–horizontal cross section of (a) vertical velocity ω, (b) streamfunction ψ, (c) temperature T, and (d) convective heating rate for wavenumber $k = 0.9$ for heating intensity $\varepsilon_T = 0.1$.

zation leads to the equation that governs the amplitude function $\Omega(p)$:

$$\frac{d^2\Omega}{dp^2} + \frac{2\lambda}{U(p) - c}\frac{d\Omega}{dp} - k^2\sigma\Omega = \frac{\varepsilon_v}{U(p_m) - c}\frac{d\Omega(p_m)}{dp}\frac{\eta(p)}{p}. \quad (27)$$

For mathematical convenience, the surface-flux damping term is not included. Jiang (1998) performed the experiment of isolating the damping effect of surface heat flux. The surface-flux damping had no significant effects on wave. The fixed, uniform stability parameter used in the present model may be the factor limiting the effect of surface-flux damping. A more detail study on the effect of surface sensible heat flux on baroclinic instability has been reported in Mak (1998).

Figure 11 gives the growth rate as a function of wavenumber for different heating intensities using the v-parameterization. As expected, the Eady case is recovered when heating is very small. As the heating intensity parameter ε_v increases, the growth rate of the unstable waves decreases. When $\varepsilon_v > 0.1$, the growth rate starts to increase, and the wavenumber of the most unstable wave shifts toward 1.5, the wavenumber of the short-wave cutoff. This is similar to the result using the *T*-parameterization. In contrast to the result using the *T*-parameterization, although the growth rate increases as ε_v becomes larger than a certain value, it does not reach the value for Eady's solution, even if heating becomes extremely large. Moreover, the real part of the wave's phase speed first decreases as ε_v increases to 0.01; then, it increases rapidly as ε_v increases from 0.01 to 1.0, eventually approaching 0.6 as ε_v increases further (not shown). The difference in phase speed leads to some difference in eigenfunctions and energy budget terms. In particular, G[CONV] remains positive as ε_v increases through the range of strong convective heating. However, the results are otherwise qualitatively the same as those using the *T*-parameterization.

Other sensitivity experiments were performed to examine the influences of cloud parameters. We changed the value of p_B while keeping $p_m = p_B$ and fixing other parameters to the reference values. The most unstable wavenumber does not change with the cloud base, and the growth rate of the most unstable wave with $\varepsilon_T = 0.1$ increases slightly from 0.145 for $p_B = 0.9$ to 0.148 for $p_B = 0.96$. When only the cloud-top changes and other parameters are fixed to the reference values, the growth rate of the most unstable wave increases as the

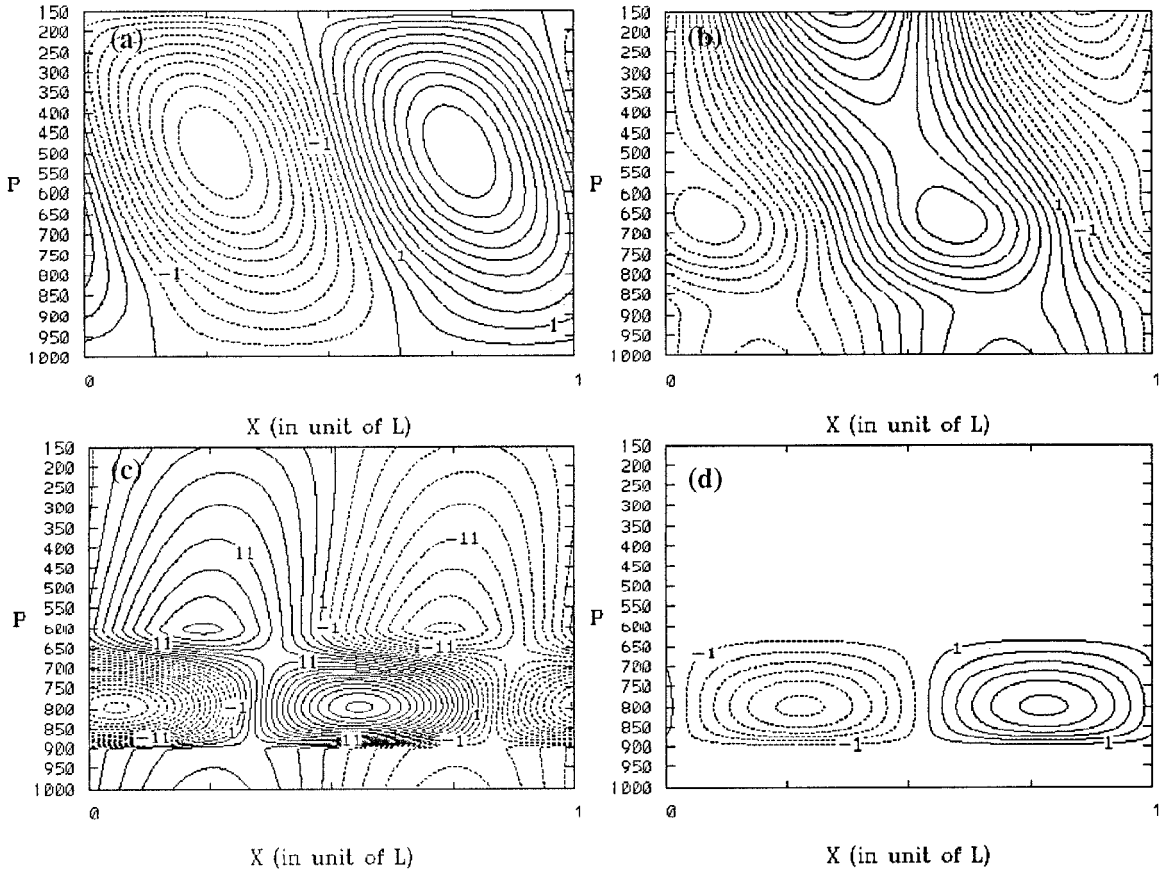

FIG. 7. Result of the *T*-parameterization model: the vertical–horizontal cross section of (a) vertical velocity ω, (b) streamfunction ψ, (c) temperature T, and (d) convective heating rate for wavenumber $k = 0.9$ for heating intensity $\varepsilon_T = 1.0$.

cloud top moves toward the surface (larger p_τ; Table 2). This behavior also occurs in Wang and Barcilon (1986). In our case, however, the most unstable wavenumber does not change with the cloud top height, which is in contrast to Wang and Barcilon (1986). Also as in Wang and Barcilon (1986), the instability changes slightly with the heating profile when the cloud top and base are fixed to the reference value (Table 3).

Because the top of the unstable PBL is not necessarily the cloud base, we also performed experiments changing p_m while fixing other parameters to the reference value. The result shows a small instability change when p_m changes from 0.85 to 0.92. Assuming that air parcels rising from the unstable boundary layer may overshoot, we allow p_m to be lower than the cloud base 0.9. How-

TABLE 1. Results of the *T*-parameterization model: phase angle difference between vertical velocity wave and temperature wave at the level where vertical velocity wave amplitude is largest.

ϵ_T	p at max (Ω)	Phase difference ($T - \Omega$)
0.0001	587.8 hPa	181.6
0.01	583.5 hPa	180.2
0.1	524.0 hPa	128.8
0.2	528.2 hPa	168.6
0.4	502.8 hPa	172.9
0.6	485.8 hPa	177.0
0.8	473.0 hPa	179.7
1.0	460.2 hPa	181.0

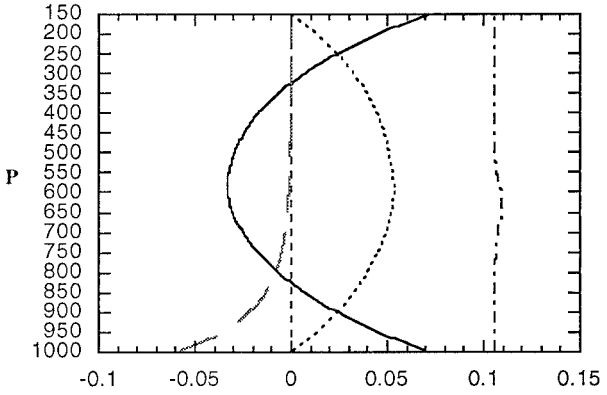

FIG. 8. Result of the *T*-parameterization model: energy budget terms of wavenumber $k = 0.9$ for $\varepsilon_T = 0.0001$. Solid line denotes DIV[EE], dotted line represents C[EPE, EKE], dash-dotted line is for C[ZPE, EPE], short dashed line for G[CONV], and long dashed line for contribution of surface damping G[DAMP].

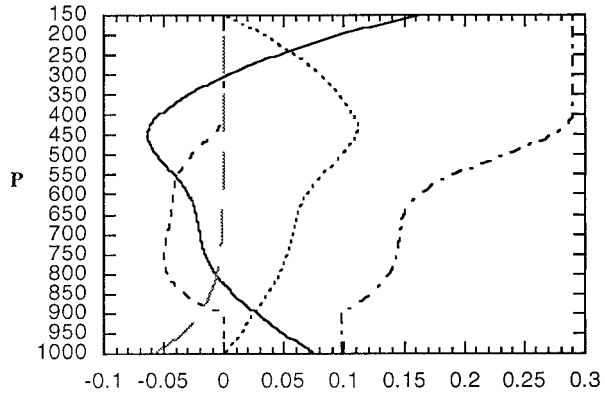

FIG. 9. Same as Fig. 8 except for $\varepsilon_T = 0.1$.

ever, considering the cloud base as the lifting condensation level and the top of the unstable PBL (p_m) as the limit of dry convection, it would be unphysical to make p_m too far below the cloud base.

4. Summary

We have used a two-dimensional, continuous model on an f plane to conduct a linear analysis of the moist instability of baroclinic zonal flow in the presence of surface–atmosphere coupling on an aquaplanet. Associated moist convective destabilization that was observed in previous work motivates parameterizing cumulus convective heating in terms of either 1) eddy temperature (T-parameterization) or 2) eddy meridional velocity (v-parameterization) at a certain level p_m, which is approximately the top of the unstable PBL, with heating in the wave's cold sector. When the model uses the T-parameterization, the surface temperature damping due to surface–atmosphere coupling is also included and assumed to decrease exponentially with height. We have derived analytically the general dispersion equation and

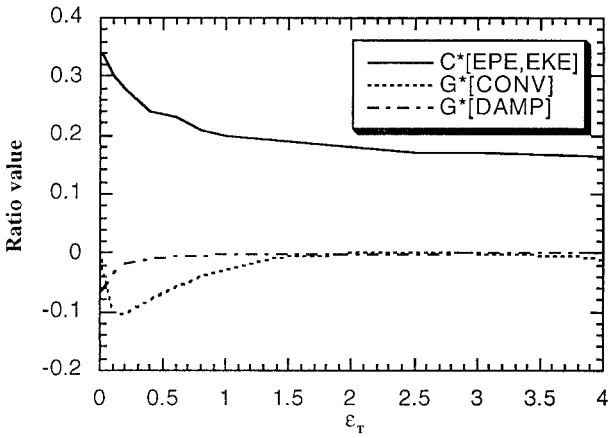

FIG. 10. Result of the T-parameterization model: the vertically integrated energy budget terms of wavenumber $k = 0.9$ for different heating intensity

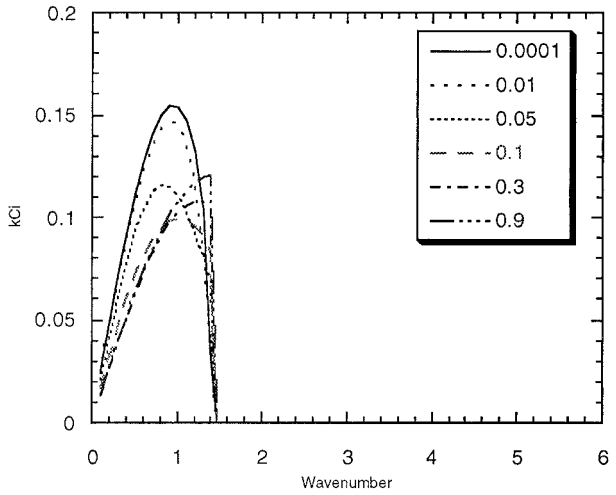

FIG. 11. Result of the v-parameterization model: variations of the growth rate with the wavenumber for different heating intensities shown in key.

eigenfunction in terms of the fundamental solutions of the homogeneous (nonheating) equation. Solutions are derived for a zonal flow with constant vertical shear, static stability, and a representative heating profile.

The T-parameterization and v-parameterization give similar results. With weak convection, the wave's structure does not change much, while the wave's energy gain is hampered by the negative contribution of convection. In the presence of moderate convective heating, although the wave's energy is decreased by the convection, the wave adjusts its structure accordingly to minimize the negative effect of convection and retain growth. In particular, the wave's temperature structure can be viewed approximately as a superpositioning of convective heating on the Eady case's temperature wave. Thus, although the wave is modified by convective heating, above and below the convective heating region, the wave structure retains features of the Eady mode.

For strong convective heating, the two parameterization schemes give somewhat different results for energetics. Using the v-parameterization, the wave's structure changes so much that the wave adapts itself to draw energy from the convective heating. With the T-parameterization scheme, convection contribution to the EPE generation becomes weakly positive when ε_T is about 2.0, but it turns negative with further increases in ε_T.

TABLE 2. Wavenumber and growth rate of the most unstable wave for each experiment, with different cloud-top level and $\epsilon_T = 0.1$.

p_T	k_{max}	g_{max}
0.3	1.0	0.133
0.4	1.0	0.145
0.5	1.0	0.155
0.6	1.0	0.160

TABLE 3. Wavenumber and growth rate of the most unstable wave for each experiment, with different heating profile and $\epsilon_T = 0.1$.

b	k_{max}	g_{max}
0.0	1.0	0.121
0.5	1.0	0.131
1.0	1.0	0.145

This study explores the instability properties and dynamics of waves interacting with wave-induced convection in the presence of surface sensible and latent heat fluxes. It does not include the potential link of surface latent heat flux to convective moistening, the wave-induced water cycle, and resulting condensational heating. In Gutowski and Jiang (1998), the wave-induced water cycle enhanced wave growth when surface latent heat flux and convective moistening were included. The lack of growth enhancement here, where the full moisture cycle is absent, is consistent with the earlier study.

Bosart and Sanders (1991) pointed out that inadequate representation of the surface sensible heat flux and related vertical transport processes could lead to occasional failure in forecasting coastal cyclogenesis. Mak (1998) emphasized the importance of adequately depicting vertical heat flux by the small-scale eddies in the boundary layer to a numerical model of marine cyclogenesis. Gutowski and Jiang (1998) and this study show that wave-induced convection related to surface sensible heat flux in the wave's cold sector also needs to be considered in investigating and forecasting marine cyclones. An implication of this study is that wave-induced convection in the cold sector modifies the wave's structure in a manner that reduces its potential negative impact on growth. This modification warrants further numerical and observational study.

Acknowledgments. We appreciate helpful comments from T.-C. Chen, G. S. Takle, R. W. Arritt, and J. L. Stanford in the course of completing this paper. We thank Chris Synder and anonymous reviewers for their thoughtful comments, which improved the clarity of this paper. This research was supported by NSF Grants ATM-913522 and ATM-9616811 to Iowa State University and by an Iowa State Office of the Provost Global-Change Assistantship.

REFERENCES

Balasubramanian, G., and M. K. Yau, 1994: Baroclinic instability in a two-layer model with parameterized slantwise convection. *J. Atmos. Sci.,* **51,** 971–990.

Bannon, P. R., 1986: Linear development of quasi-geostrophic baroclinic disturbances with condensational heating. *J. Atmos. Sci.,* **43,** 2261–2274.

Bosart, L., and F. Sanders, 1991: An early-season coastal storm: Conceptual success and model failure. *Mon. Wea. Rev.,* **119,** 2831–2851.

Charney, J. G., 1947: The dynamics of long waves in a baroclinic westerly current. *J. Meteor.,* **4,** 135–163.

Eady, E. T., 1949: Long waves and cyclone waves. *Tellus,* **1,** 33–52.

Emanuel, K. A., 1991: A scheme for representing cumulus convection in large-scale models. *J. Atmos. Sci.,* **48,** 2313–2335.

——, M. Fantini, and A. J. Thorpe, 1987: Baroclinic instability in an environment of small stability to slantwise moist convection. Part I: Two-dimensional models. *J. Atmos. Sci.,* **44,** 1559–1573.

Fantini, M., 1990: Nongeostrophic corrections to the eigensolutions of a moist baroclinic instability problem. *J. Atmos. Sci.,* **47,** 1277–1287.

——, 1995: Linear baroclinic instability in the presence of heat inflow from the lower boundary. *Ann. Geophys.,* **13,** 419–426.

Farrell, B. F., 1982: The initial growth of disturbances in a baroclinic flow. *J. Atmos. Sci.,* **39,** 1663–1686.

Gutowski, W. J., and W. Jiang, 1998: Surface-flux regulation of the coupling between cumulus convection and baroclinic waves. *J. Atmos. Sci.,* **55,** 940–953.

Jiang, W., 1998: Coupling of baroclinic waves, cumulus convection, and surface processes. Ph.D. thesis, Dept. of Geological and Atmospheric Sciences, Iowa State University, 127 pp. [Available from UMI, P.O. Box 1346, Ann Arbor, MI 48106-1346; available online from http://www.umi.com.]

Lindzen, R. E., 1974: Wave-CISK in the tropics. *J. Atmos. Sci.,* **31,** 156–179.

Mak, M., 1982: On moist quasi-geostrophic baroclinic instability. *J. Atmos. Sci.,* **39,** 2028–2037.

——, 1983: On moist quasi-geostrophic baroclinic instability in a general model. *Sci. Sin.,* **26B,** 850–864.

——, 1994: Cyclogenesis in a conditionally unstable moist baroclinic atmosphere. *Tellus,* **46A,** 14–33.

——, 1998: Influence of surface sensible heat flux on incipient marine cyclogenesis. *J. Atmos. Sci.,* **55,** 820–834.

Moorthi, S., and A. Arakawa, 1985: Baroclinic instability with cumulus heating. *J. Atmos. Sci.,* **42,** 2007–2031.

Olafsson, H., and H. Okland, 1994: Precipitation from convective boundary layers in arctic air masses. *Tellus,* **46A,** 4–13.

Orlanski, I., 1986: Localized baroclinicity: A source for meso-α cyclones. *J. Atmos. Sci.,* **43,** 2857–2885.

Tokioka, T., 1973: A stability study of medium-scale disturbances with inclusion of convective effects. *J. Meteor. Soc. Japan,* **51,** 1–10.

Wang, B., and A. Barcilon, 1986: Moist stability of a baroclinic zonal flow with conditionally unstable stratification. *J. Atmos. Sci.,* **43,** 705–719.